

Dust and Polycyclic Aromatic Hydrocarbon in the HD 34700 Debris Disk

Ji Yeon Seok and Aigen Li

Department of Physics and Astronomy, University of Missouri, Columbia, MO 65211, USA; seokji@missouri.edu, lia@missouri.edu

ABSTRACT

The debris disk around the Vega-type star HD 34700 is detected in dust thermal emission from the near infrared (IR) to millimeter (mm) and submm wavelength range. Also detected is a distinct set of emission features at 3.3, 6.2, 7.7, 8.6, 11.3 and 12.7 μm , which are commonly attributed to polycyclic aromatic hydrocarbon (PAH) molecules. We model the observed dust IR spectral energy distribution (SED) and PAH emission features of the HD 34700 disk in terms of porous dust and astronomical-PAHs. Porous dust together with a mixture of neutral and ionized PAHs closely explains the dust IR SED and PAH emission features observed in the HD 34700 disk. Due to the stellar radiation pressure and Poynting–Robertson drag together with the photodissociation of PAHs, substantial removal of dust and PAHs has occurred in the disk, and continuous replenishment of these materials is required to maintain their current abundances. This implies that these materials are not primitive but secondary products probably originating from mutual collisions among planetesimals, asteroids, and comets.

Subject headings: circumstellar matter — infrared: stars — stars: individual: HD 34700

1. Introduction

Vega-type stars are main-sequence (MS) stars with infrared (IR) emission in excess of the stellar photospheric radiation (see Backman & Paresce 1993). This “excess” emission is attributed to the thermal emission of solid dust grains in a “debris” disk, an optically thin disk orbiting around the central star. In debris disks, the gas is tenuous, and dust grains are removed easily by radiation pressure (RP) and the Poynting–Robertson drag (Burns et al. 1979, Backman & Paresce 1993). To sustain a debris disk, dust grains need to be replenished continuously by collisions between planetesimals, asteroids, and comets. This

implies that grains in a debris disk are not the primordial materials left over from the protostellar molecular cloud but remnants of the planet formation process.

HD 34700, also known as SAO 112630, is classified as a Vega-like star based on its IR excess (e.g., see Walker & Wolstencroft 1988). It has a spectral type of G0 IVe, an effective temperature of $T_{\text{eff}} \approx 6000$ K (see Schütz et al. 2009 and references therein), and a total stellar luminosity of $L_{\star} \approx 20.4 L_{\odot}$ (Acke & van den Ancker 2004). With a Hipparcos parallax of $\approx 0.86 \pm 1.84$ mas, its distance d is very uncertain, which makes the estimate of its age, mass, and size ambiguous. It has been suggested that d is at least ~ 100 pc (Torres 2004), and its apparent proximity to Orion provides an upper limit of $d \sim 430$ pc. Assuming $d \approx 200$ pc, Torres (2004) estimated the stellar mass to be $M_{\star} \approx 1.1\text{--}1.2 M_{\odot}$.

The HD 34700 system is known as a multiple system consisting of a spectroscopic binary (Torres 2004) and two other faint stellar components which are at a separation of $\sim 5''.2$ and $\sim 9''.2$, respectively, for Component B and Component C (Sterzik et al. 2005). While the two faint components are classified as bonafide T Tauri stars (TTS) based on their strong H α emission and Li I $\lambda 6798$ absorption, the nature of the spectroscopic binary is somewhat vague. Both the H α emission and the Li I $\lambda 6798$ absorption (with an equivalent width of ~ 0.6 and ~ 0.17 Å, respectively) detected in HD 34700 are relatively weak (Arellano Ferro & Giridhar 2003, Sterzik et al. 2005), indicating that the age of HD 34700 cannot be a few mega-years but a few tens of mega-years (Torres 2004). Moreover, as we will show later in Section 5 that the lifetime of the dust grains in the disk around HD 34700 is shorter than the stellar age, therefore it is plausible that HD 34700 has a debris disk rather than a protoplanetary disk.

The HD 34700 debris disk has been extensively studied observationally, including space-borne and ground-based broadband photometry of the IR “excess” emission from the near-IR to submillimeter wavelengths. Of particular interest is the detection of the prominent 3.3, 6.2, 7.7, 8.6, and 11.3 μm emission bands in HD 34700. These emission features are collectively known as the “unidentified infrared” (UIR) emission bands (see Tielens 2008, Peeters 2014, Joblin 2015) and are now generally attributed to polycyclic aromatic hydrocarbon (PAH) molecules (Léger & Puget 1984; Allamandola et al. 1985). They are ubiquitously seen in a wide variety of Galactic and extragalactic regions, including protoplanetary disks around Herbig Ae/Be stars and TTS and disks in transition from a primordial to debris phase (e.g., see Brooke et al. 1993, Siebenmorgen et al. 2000, Acke & van den Ancker 2004, van Boekel et al. 2004, Geers et al. 2005, Sloan et al. 2005, Weinberger & Becklin 2005, Furlan et al. 2006, Habart et al. 2006, Keller et al. 2008). However, the detection of the PAH emission features in debris disks is relatively rare. To the best of our knowledge, they are reportedly seen in only a few debris disks (Coulson & Walther 1995, Sylvester et al. 1997, Smith et al.

2004). For example, Acke et al. (2010) found that 37 out of 53 Herbig Ae/Be stars show PAH features in their IR spectra obtained with the *Infrared Spectrograph* (IRS) on board the *Spitzer Space Telescope*. In contrast, Chen et al. (2006) reported no detection of PAH emission in the *Spitzer*/IRS spectra of 59 MS stars classified as Vega-like objects based on the *IRAS* 60 μm excess.

PAHs play an important role in gas-rich planet-forming disks. They dominate the heating of the gas in their surface layers. They are also diagnostic of the presence of very small grains in their surface layers, which in return are diagnostic of the settling and coagulation processes occurring in the disks that ultimately lead to the formation of planetesimals (see J. Y. Seok & A. Li 2015, in preparation). For gas-depleted debris disks, PAHs could potentially be used to probe their disk structures that are widely considered as signposts for planet formation. Due to their stochastic heating nature (see Draine & Li 2001), the PAH emission features are expected to be spatially more extended than the emission of large grains that are in thermal equilibrium with the stellar radiation. Therefore, debris disks could be more easily resolved at the PAH emission bands.

The 3.3 μm PAH C–H stretching feature was clearly detected in the $\sim 1.9\text{--}4.2\ \mu\text{m}$ spectrum of HD 34700 obtained with the medium-resolution spectrograph *SpeX* at the NASA *Infrared Telescope Facility* (IRTF; Smith et al. 2004). The 6.2 and 7.7 μm C–C stretching features as well as the 11.3 μm out-of-plane C–H bending feature were detected in the $\sim 2.5\text{--}12\ \mu\text{m}$ spectrum of HD 34700 obtained by the spectrophotometer *ISOPHOT* on board the *Infrared Space Observatory* (ISO) albeit its limited spectral resolution of $\lambda/\Delta\lambda \approx 90$ (Acke & van den Ancker 2004), and later by *Spitzer*/IRS with higher sensitivities (Berné et al. 2009, Schütz et al. 2009). By combining the *ESO*/TIMMIS2 $\sim 8\text{--}13\ \mu\text{m}$ N-band spectrum with the *Spitzer*/IRS spectrum, Schütz et al. (2009) also reported marginal detections of the 8.6 μm C–H in-plane bending feature and the 12.7 μm out-of-plane C–H bending feature.

With a distinct set of prominent PAH emission features detected, HD 34700 offers a rare opportunity to explore the nature and origin of PAHs in debris disks. In this work we model the dust and PAH emission of the HD 34700 debris disk, with an aim of exploring its dust and PAH properties. This paper is organized as follows. We describe the observational data of dust and PAH emission in Section 2. We present the PAH and dust models in Section 3. The results are summarized in Section 4 and discussed in Section 5 with special attention paid to the photophysics of PAHs. The major conclusions are summarized in Section 6.

Table 1. Photometric Data for the HD 34700 System

Telescope /Mission	Wavelength (μm)	Flux Density (Jy)	Uncertainty (Jy)
EXPORT	0.36 (<i>U</i>)	0.239	0.0088
	0.44 (<i>B</i>)	0.578	0.0267
	0.53 (<i>V</i>)	0.887	0.0409
	0.69 (<i>R</i>)	0.941	0.0780
	0.83 (<i>I</i>)	0.887	0.0818
2MASS	1.235 (<i>J</i>)	0.968	0.0205
	1.662 (<i>H</i>)	0.847	0.0179
	2.159 (<i>K_S</i>)	0.678	0.0150
<i>WISE</i>	3.4	0.467	0.014
	4.6	0.327	0.005
	12	0.422	0.004
	22	3.33	0.02
<i>AKARI</i>	9	0.51	0.012
	18	1.76	0.03
	65	12.5	0.8
	90	10.9	0.6
	140	5.34	1.0
<i>IRAS</i>	12	0.605	0.0424
	25	4.42	0.309
	60	14.1	1.41
	100	9.38	0.938
SCUBA	450	0.218	0.037
	850	0.041	0.0024
	1100	0.039	0.013
	1350	0.0117	0.0011

Note. — The EXPORT *UBVRI*, *IRAS*, and SCUBA fluxes are taken from Mendigutía et al. (2012). The 2MASS, *WISE*, and *AKARI* photometric fluxes are extracted from the online catalogs.

2. Data

We compile all the photometric data for HD 34700 available in the literature. The *UBVRI*, *IRAS*, and *SCUBA* fluxes are taken from Mendigutía et al. (2012) and references therein. The near- to far-IR fluxes are extracted from the 2MASS *All-sky Point Source Catalog*,¹ the *WISE All-sky Source Catalog*,² the *AKARI Infrared Camera (IRC) All-sky Survey Point Source Catalogue* (Version 1.0, Ishihara et al. 2010), and the *AKARI Far Infrared Surveyor (FIS) All-sky Survey Bright Source Catalogue* (Version 1.0).³ All the photometric fluxes and uncertainties reported in the literature are summarized in Table 1. For the spectroscopic data of HD 34700, we adopt the $\sim 1.9\text{--}4.2\ \mu\text{m}$ *IRTF*/SpeX spectrum of Smith et al. (2004) and the $\sim 5\text{--}14\ \mu\text{m}$ *Spitzer*/IRS spectrum of Schütz et al. (2009). A combination of both photometric and spectroscopic data enables us to perform a comprehensive modeling of the observed spectral energy distribution (SED) to examine all the major PAH features from ~ 3 to $\sim 14\ \mu\text{m}$ as well as the dust properties simultaneously.

Figure 1(a) shows the broadband photometry of HD 34700 together with the *IRTF*/SpeX and *Spitzer*/IRS spectra. In addition, we plot the Kurucz stellar atmospheric model spectrum for $T_{\text{eff}} = 6000\ \text{K}$ and a surface gravity of $\lg g = 4.0$ (Kurucz 1979). To correct for the interstellar extinction, the knowledge of the visual extinction (A_V) toward HD 34700 is required. In the literature, a range of A_V values has been reported (e.g., $A_V \approx 0\text{--}0.68\ \text{mag}$, Coulson et al. 1998, van den Ancker 1998, Acke & van den Ancker 2004), but it is as uncertain as its distance. In modeling the observed SED, we set the distance d and visual extinction A_V as free parameters. We search for the best values that reproduce the photometric fluxes with the Kurucz model. It is found that $d \approx 260\ \text{pc}$ and $A_V \approx 0.5\ \text{mag}$ closely reproduce the photometric fluxes in the ultraviolet/optical and near-IR bands. Therefore, we adopt $d = 260\ \text{pc}$ with $A_V = 0.5\ \text{mag}$ for further analysis in this work.⁴

Figures 1(b),(c) focus on the $3.3\ \mu\text{m}$ PAH feature and the PAH features at longer wavelengths, respectively. It is interesting to note that the $3.3\ \mu\text{m}$ aromatic C–H stretch feature of HD 34700 is accompanied by a weaker feature at $3.43\ \mu\text{m}$ (see Figure 1(b)), which is generally ascribed to aliphatic C–H stretch (Joblin et al. 1996, Li & Draine 2012, Yang et al. 2013).

¹<http://www.ipac.caltech.edu/2mass/releases/allsky>

²<http://wise2.ipac.caltech.edu/docs/releases/allsky>

³<http://www.ir.isas.jaxa.jp/AKARI/Observation/PSC/Public>

⁴If $A_V = 0$, the same Kurucz model with $d \approx 320\ \text{pc}$ can also closely reproduce the photometric fluxes up to the *J*, *H*, *K_s* bands but is deficient in the *WISE* 3.4 and $4.6\ \mu\text{m}$ bands. If this true, the excess emission at the *WISE* 3.4 and $4.6\ \mu\text{m}$ bands may indicate the existence of an inner, warm “zodiacal cloud” in the HD 34700 disk.

In addition to the $3.43\,\mu\text{m}$ C–H stretch, aliphatic hydrocarbon materials also have two C–H deformation bands (see Li & Draine 2012). The *Spitzer*/IRS spectrum of HD 34700 reveals the presence of these two features at ~ 6.89 and $\sim 7.23\,\mu\text{m}$ (see Figure 1(c)). Compared with the PAH features seen in the diffuse ISM (e.g., see Tielens 2008), the $7.7\,\mu\text{m}$ feature is somewhat red-shifted and appreciably broadened, while the $8.6\,\mu\text{m}$ feature is much weaker. These characteristics belong to either class B or C following the PAH spectral classification of Peeters et al. (2002), which is typically found in planetary nebulae and isolated Herbig Ae/Be stars.

3. Model

To simultaneously model the dust emission and the *IRTF*/SpeX and the *Spitzer*/IRS spectra, we adopt the porous dust model of Li & Lunine (2003a) and the astro-PAH model of Li & Draine (2001) and Draine & Li (2007).

3.1. PAHs

Following Li & Draine (2001) and Li & Lunine (2003a), we assume a log-normal size distribution for the PAHs in the HD 34700 disk. The log-normal size distribution function is characterized by two parameters, a_0 and σ , which determine the peak location and the width of the log-normal distribution, respectively:

$$dn_{\text{PAH}}/da = \frac{1}{\sqrt{\pi/2}\sigma \{1 - \text{erf} [\ln(a_{\text{min}}^{\text{PAH}}/a_0)/\sqrt{2}\sigma]\}} \frac{1}{a} \exp \left\{ -\frac{1}{2} \left[\frac{\ln(a/a_0)}{\sigma} \right]^2 \right\}, \text{ for } a > a_{\text{min}}^{\text{PAH}}. \quad (1)$$

We set the lower cutoff of the PAH size as $a_{\text{min}}^{\text{PAH}} \equiv 3.5\,\text{\AA}$ corresponding to ~ 20 carbon atoms in a PAH molecule (i.e., $N_{\text{C}} \approx 20$), which is the minimum survival size for PAHs in the diffuse ISM (see Li & Draine 2001). We treat a_0 and σ as free parameters. The total PAH mass will be derived from fitting the observed PAH emission features.

For the PAH absorption cross sections, we adopt those of Draine & Li (2007). Two types of PAHs are distinguished: neutral PAHs and charged PAHs. For charged PAHs, we do not distinguish either cations from anions or multiply charged PAHs from singly charged PAHs.

The astro-PAH model of Li & Draine (2001) and Draine & Li (2007) represents the absorption cross section of each PAH feature by a Drude profile, which is expected for classical damped harmonic oscillators (see Li 2009a). Drude profiles are characterized by

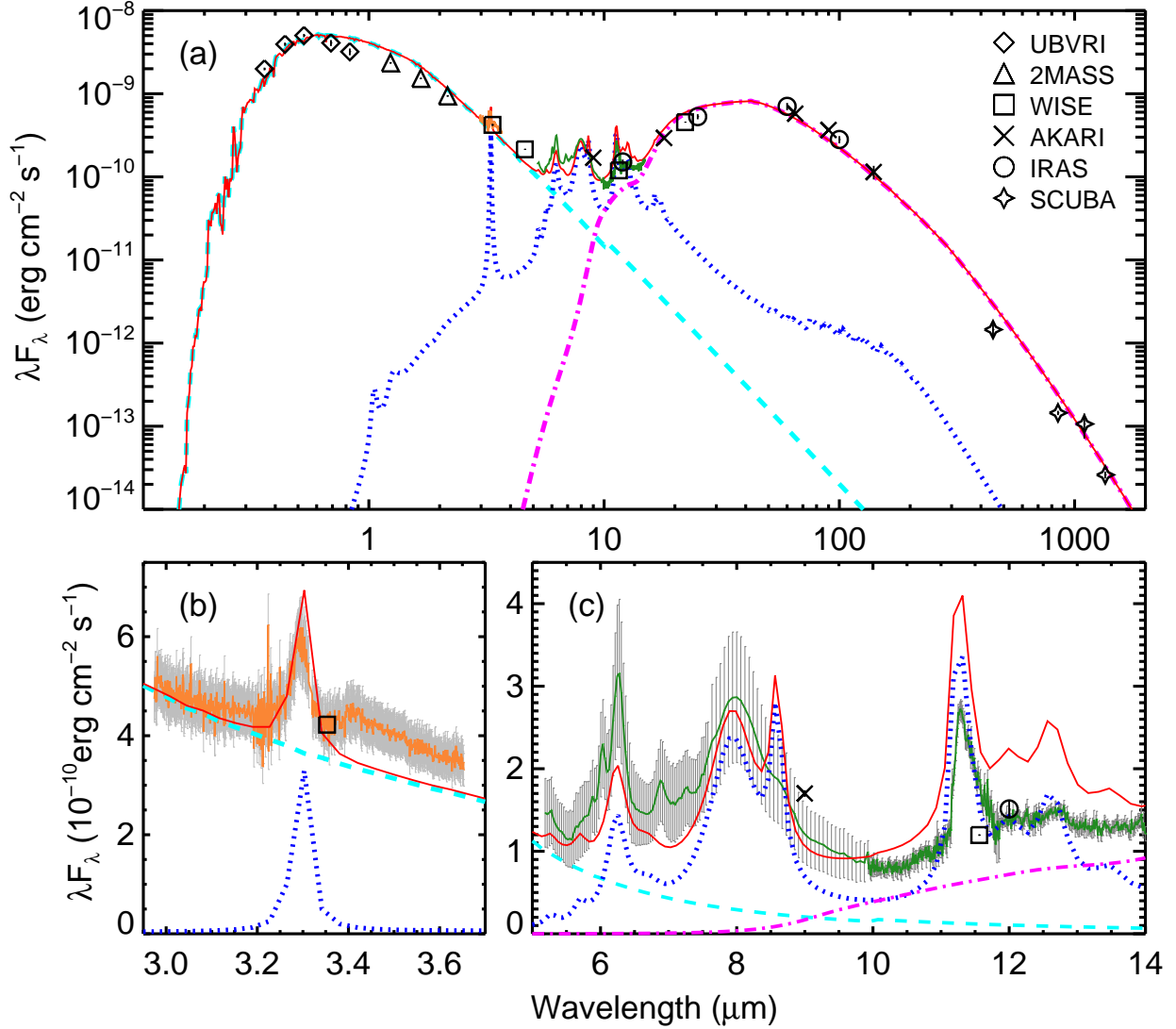


Fig. 1.— (a) Spectral energy distribution of HD 34700. The photometric fluxes are shown with symbols (see Table 1). The near-IR *IRTF*/SpeX spectrum (Smith et al. 2004) and mid-IR *Spitzer*/IRS spectrum (Schütz et al. 2009) are shown as the orange and green lines, respectively. The photometric uncertainties are overlaid although most of them are smaller than the size of the symbols. Our best-fit model spectrum is presented as the red solid line, which is composed of the stellar (cyan dashed line), PAHs (blue dotted line), and dust (magenta dashed-dotted line) components. (b)–(c) Same as panel (a), but enlarged views of the *IRTF*/SpeX spectrum and the *Spitzer*/IRS spectrum of HD 34700, respectively, with measured uncertainties overlaid (gray).

their peak wavelengths, widths, and strengths (i.e., the wavelength-integrated absorption cross sections). As mentioned earlier (see Section 2), the PAH feature profiles detected in HD 34700 somewhat differ from those typically seen in the diffuse ISM. In modeling the PAH emission features of HD 34700, we slightly adjust the peak wavelength and width for several features, but with the strength fixed. We note that it is not unphysical to adjust the peak wavelength and width as long as the strength is unaltered.

We will only model the major PAH features such as those at 3.3, 6.2, 7.7, 8.6 and 11.3 μm . Nevertheless, the intensities of the minor, aliphatic C–H features at 3.43, 6.89, and 7.23 μm are measured and will be briefly discussed in Section 5.1. The aliphatic C–H features of HD 34700 and other disks will be fully investigated in a separate paper (J. Y. Seok & A. Li 2015, in preparation).

The PAH features shown in Figure 1 manifest that both neutral and ionized PAHs exist in the HD 34700 disk because ionized PAHs emit strongly at 6.2, 7.7, and 8.6 μm , in contrast, neutral PAHs emit strongly at 3.3 and 11.3 μm . The charge distribution of PAHs is determined by the balance between the photoionization and the electron recombination (Bakes & Tielens 1994, Weingartner & Draine 2001), which is proportional to $U\sqrt{T_{\text{gas}}}/n_e$, where U is the ultraviolet (UV) starlight intensity, T_{gas} is the gas temperature, and n_e is the electron density. Moreover, the PAH size also affects its charging. Following the approaches described in Li & Lunine (2003a), we calculate the photoionization rate (k_{ion}) and the electron recombination rate (k_{rec}) for PAHs of a given size at a given distance (r) from the central star (see Appendices A and B in Li & Lunine 2003a).

To calculate k_{rec} , we need to know the electron density n_e as a function of r , the distance from the central star. We assume the cosmic-ray ionization of H_2 to be the major source of the electrons in the HD 34700 disk. The electron density is derived from $n_e \approx \tau_\star \varsigma_{\text{CR}} n_{\text{H}_2}$, where $\varsigma_{\text{CR}} \approx 3 \times 10^{-17} \text{ s}^{-1}$ is the cosmic ionization rate and $\tau_\star \approx 10 \text{ Myr}$ is the stellar age. We obtain n_{H_2} from $M(\text{H}_2)$, the total mass of H_2 in the HD 34700 disk. We adopt $M(\text{H}_2) = 1502 M_\oplus$ after scaling the original value of $M(\text{H}_2) \approx 80 M_\oplus$ at $d \approx 60 \text{ pc}$ of Zuckerman et al. (1995) to $d \approx 260 \text{ pc}$, the distance adopted in this work. Assuming a vertical hydrostatic equilibrium for the disk (see Equations (B2)–(B4) in Li & Lunine 2003a), we derive $n_{\text{H}_2}(r)$, the spatial distribution of H_2 , and then n_e (see Figure 2(a)). Also, we take $T_{\text{gas}}(r) \approx (R_\star/2r)^{1/2} T_{\text{eff}} \approx 591 (r/\text{AU})^{-1/2} \text{ K}$, where $R_\star \approx 0.0194 \text{ AU}$ is the stellar radius (see Figure 2(b)). In Figure 2(d), we show the ionization parameter $U\sqrt{T_{\text{gas}}}/n_e$ as a function of the distance r from the central star, where the starlight intensity, U , is in unit of the 912 Å–1 μm local interstellar radiation field of Mathis et al. (1983; MMP83).

In Figure 3(a), the photoionization timescales ($\tau_{\text{ion}} \equiv 1/k_{\text{ion}}$) and the electron recombination timescales ($\tau_{\text{rec}} \equiv 1/k_{\text{rec}}$) as a function of PAH size are depicted for given distances

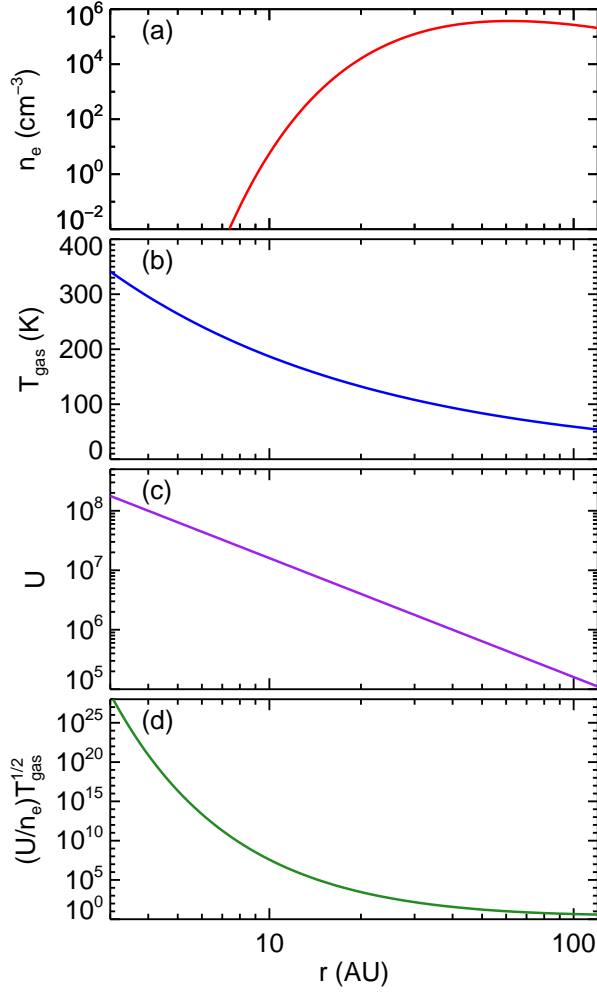


Fig. 2.— Radial profiles of (a) the electron density, n_e (cm^{-3}), (b) the gas temperature, T_{gas} (K), (c) the starlight intensity, U , in unit of the 912 \AA – $1 \mu\text{m}$ MMP83 ISRF (e.g., see Equation (1) of Li & Lunine 2003a), and (d) the ionization parameter $U\sqrt{T_{\text{gas}}/n_e}$ as a function of distance, r (AU), from the central star in the HD 34700 disk. Since the ionization balance of PAHs is controlled by $U\sqrt{T_{\text{gas}}/n_e}$ (Bakes & Tielens 1994, Weingartner & Draine 2001), the trend seen in panel (d) depicts the overall charging of PAHs depending on the distance to the central star.

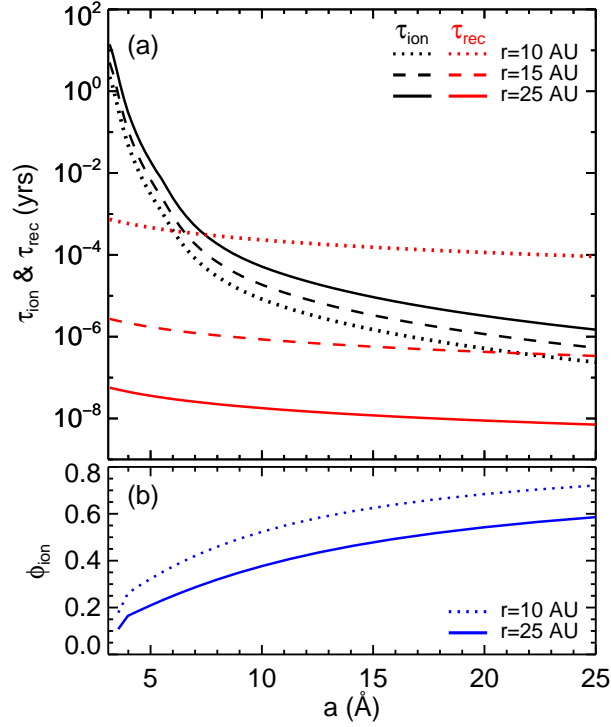


Fig. 3.— Upper panel (a) Photoionization (τ_{ion}) and electron recombination (τ_{rec}) timescales for PAHs in the size range of $3.5 \text{ \AA} < a < 25 \text{ \AA}$ at $r = 10$ AU (dotted lines), 15 AU (dashed lines), and 25 AU (solid lines) from the central star. In calculating τ_{rec} , we estimate n_e from $M(\text{H}_2)$, the mass of H_2 determined by Zuckerman et al. (1995), assuming that the cosmic-ray ionization of H_2 is the dominant contributor to the electrons in the HD 34700 disk. Lower panel (b) ionization fraction (ϕ_{ion}) of PAHs as a function of size at $r = 10$ and 25 AU.

from the central star ($r = 10, 15$, and 25 AU). Note that $r = 25$ AU is considered to be the cutoff distance of the PAH distribution in the HD 34700 disk since at $r > 25$ AU the dust temperatures drop to $T < 120$ K (see Section 4), so the dust will acquire an ice mantle and PAHs will condense onto the ice mantle. As discussed in Li & Lunine (2003a), τ_{ion} decreases for larger PAHs since the ionization threshold is inversely proportional to the PAH size. Also, τ_{ion} decreases as PAHs get closer to the central star. This is because the starlight intensity is enhanced (i.e., $U \propto r^{-2}$, see Figure 2(c)).

In comparison with τ_{ion} , τ_{rec} is found to be much shorter than τ_{ion} at $r = 25$ AU whereas τ_{rec} becomes comparable to τ_{ion} at $r \simeq 15$ AU for large PAHs. At $r = 10$ AU, PAHs with $a \gtrsim 6$ Å have τ_{ion} even shorter than τ_{rec} . This indicates that PAHs, in particular large PAHs, can attain an ionized state in the inner region while PAHs in the outer region are more likely to be neutral (or negatively charged).

Using the photoelectric emission and electron capture rates of Weingartner & Draine (2001), we investigate the PAH charging process in the HD 34700 disk. At a given distance from the star, we calculate the ionization fraction (ϕ_{ion}) of PAHs as a function of PAH size, which is the probability of finding a PAH molecule in a nonzero charge state. As shown in Figure 3(b) for $\phi_{\text{ion}}(a)$ at $r = 10$ and 25 AU, small PAHs are more likely to be neutral, and large PAHs are more likely to be ionized. This is consistent with the comparison between the photoionization and electron recombination timescales (see Figure 3(a)). Overall, ϕ_{ion} decreases as the distance r increases, consistent with the variation trend of $U\sqrt{T_{\text{gas}}}/n_{\text{e}}$ with r (see Figure 2(d)) which determines the charging of PAHs as a function of r . Roughly speaking, PAHs near the central star are fully ionized since $\tau_{\text{ion}} \ll \tau_{\text{rec}}$ even for the smallest PAHs. At ~ 15 – 25 AU, however, because of $\tau_{\text{ion}} \gtrsim \tau_{\text{rec}}$ for PAHs of $a \lesssim 20$ Å (see Figure 3(a)), a fraction of them will be negatively charged, so ϕ_{ion} will be nonzero even for the smallest PAHs at $r = 25$ AU (see Figure 3(b)). Therefore, we expect a mixture of neutral and charged PAHs (cations or anions) in the HD 34700 disk. Note that, following Li & Draine (2001), we do not distinguish cations and anions when we model the IR emission of PAHs.

3.2. Dust

The porous grain model of Li & Lunine (2003a) for protoplanetary and debris disks assumes that the dust consists of porous aggregates of amorphous silicate and carbonaceous materials, and the dust in regions cooler than ~ 120 K is further coated with H_2O -dominated ices. We take the dielectric functions of “astronomical” silicate of Draine & Lee (1984) for the silicate component, amorphous carbon of Rouleau & Martin (1991) for the carbonaceous component, and “dirty” ice of Li & Greenberg (1998) for the ice component. Assuming

a spherical shape, the absorption cross sections of porous dust are calculated from Mie theory combined with the Maxwell–Garnett and Bruggeman effective medium theories (see Li 2009a). We adopt the mass mixing ratios of Li & Lunine (2003b) derived from cosmic abundance considerations. We first employ the Maxwell-Garnett effective medium theory to calculate the average dielectric functions for the ice-coated silicate subgrains and the ice-coated carbonaceous subgrains (see Equations (7), (8) of Li & Lunine 2003a) and then use the Bruggman effective medium theory to calculate the average dielectric functions for the porous dust aggregate (Equation (9) of Li & Lunine 2003a). The porosity (or fluffiness) of a grain is quantified by the fractional volume of vacuum (P). Following Li & Lunine (2003a, 2003b), we adopt $P = 0.90$ for porous dust and $P' \approx 0.73$ for the ice-coated porous dust, and the choice of P will be discussed in Section 4.

For the spherical dust, we adopt a power-law size distribution: $dn/da \propto a^{-\alpha}$, where a is the spherical radius of the dust, and α is the power-law index. We take the lower cutoff size to be $a_{\min} = 1 \mu\text{m}$ and the upper cutoff size to be $a_{\max} = 1 \text{ cm}$. Li & Lunine (2003a) have shown that changing a_{\min} and a_{\max} does not significantly alter the model-fitting. This will be discussed in Section 4. We vary α from 0.1 to 4.0 to search for the best fit.

For the spatial (radial) distribution of the dust in the HD 34700 disk, instead of using a simple power-law with sharp inner and outer boundary cutoffs, we propose a more physical formula for the spatial distribution, which is defined as

$$\frac{dn}{dr} \propto \left(1 - \frac{r_{\min}}{r}\right)^{\beta} \left(\frac{r_{\min}}{r}\right)^{\gamma}, \quad (2)$$

where r_{\min} is the inner boundary of the disk, which is set to be the distance where the dust temperature reaches $\sim 1500 \text{ K}$ and dust sublimates. This functional form has the advantage that on one hand, it resembles a power-law $dn/dr \propto r^{-\gamma}$ at larger distances ($r \gg r_{\min}$), and on the other hand it peaks at $r_p = r_{\min} (\beta + \gamma) / \gamma$, unlike the simple power-law which peaks at r_{\min} . The latter is unphysical as it assumes that the dust piles up at r_{\min} where dust actually sublimates. We take $r_{\min} = 0.3 \text{ AU}$ since the equilibrium temperature of micrometer-sized dust reaches $\sim 1500 \text{ K}$ at $r \sim 0.3 \text{ AU}$ from the central star. We take the outer disk boundary to be $r_{\max} = 1000 \text{ AU}$. Our model is not sensitive to r_{\max} , but $r_{\max} = 1000 \text{ AU}$ is a reasonable assumption in view of the distance to the nearest companion star in the system of HD 34700.⁵ In summary, we have two free parameters, r_p and γ , for the dust spatial distribution.

⁵The angular distance from the central star to the stellar component B is $\sim 5''.2$ (Sterzik et al. 2005), which corresponds to $\sim 1350 \text{ AU}$ at a distance of $d = 260 \text{ pc}$.

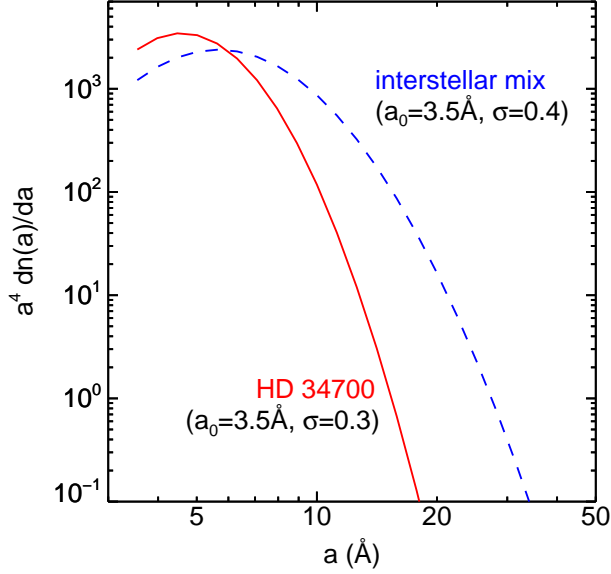


Fig. 4.— Log-normal size distribution for the PAH population. The best-fit model with $a_0 = 3.5 \text{ \AA}$ and $\sigma = 0.3$ is compared with that of the interstellar PAH model ($a_0 \approx 3.5 \text{ \AA}$ and $\sigma \approx 0.4$, Li & Draine 2001). The size distribution is expressed by multiplying a^4 to show the mass distribution per logarithmic PAH radius.

4. Results

Figure 1 shows our best-fit model that reasonably reproduces all the observational data. The best-fit model includes emission from a mixture of neutral/ionized PAHs and porous dust with a power-law size distribution index of $\alpha \approx 3.5$ and a total dust mass of $M_{\text{dust}} \approx 21.9 M_{\oplus}$. The disk geometry is characterized with $r_p \approx 100 \text{ AU}$ and $\gamma \approx 2$ (see Equation (2)). The PAH component is determined by $a_0 \approx 3.5 \text{ \AA}$ and $\sigma \approx 0.3$, and the total PAH mass is $M_{\text{PAH}} \approx 4.53 \times 10^{-7} (r/\text{AU})^2 M_{\oplus}$ if all PAHs are at a distance of r from the central star. We do not have any prior information how the PAHs are spatially distributed in the HD 34700 disk. Due to their stochastic heating nature (Draine & Li 2001), the PAH emission spectral profiles do not vary with the starlight intensity. Therefore, the PAH emission features should essentially remain identical for PAHs at different distances from the central star, except that the flux level scales with r^{-2} . Consequently, the PAH mass required to account for the observed PAH emission features scales with r^2 .

The PAH size distribution with the best fit parameters is shown in Figure 4 together with that of the interstellar mixture (i.e., $a_0 \approx 3.5 \text{ \AA}$ and $\sigma \approx 0.4$, Li & Draine 2001). Compared with the diffuse ISM, the PAH emission features observed in the HD 34700 disk are in favor of smaller PAHs.

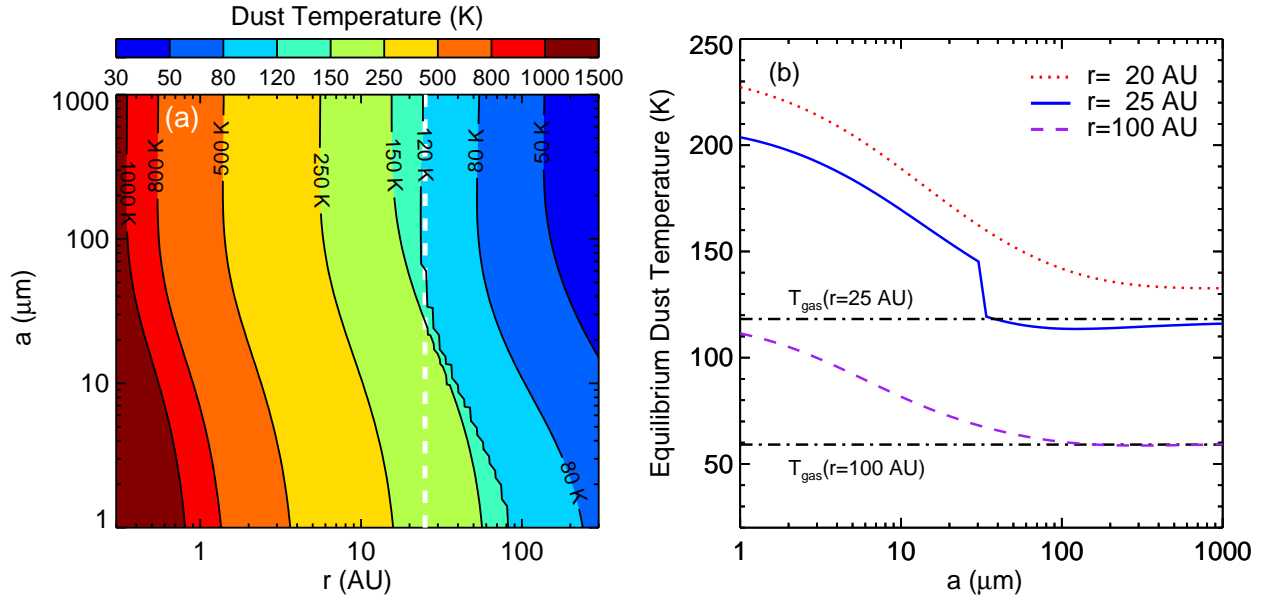


Fig. 5.— (a) Temperatures of porous dust (of porosity $P = 0.90$ for $T > 120 \text{ K}$ and $P' = 0.73$ for $T < 120 \text{ K}$) as a function of grain size (a) and radial distance (r) from the central star. (b) Temperatures of porous dust as a function of grain size at $r = 20 \text{ AU}$ (dotted lines), $r = 25 \text{ AU}$ (solid lines), and $r = 100 \text{ AU}$ (dashed lines). A sudden temperature drop around $a \approx 30 \mu\text{m}$ is caused by the ice sublimation at $T \approx 120 \text{ K}$. For comparison, the gas temperatures $T_{\text{gas}} \approx 591 (r/\text{AU})^{-1/2} \text{ K}$ at the same distances are overlaid.

Our model yields a total dust IR flux of $\int_{912\text{\AA}}^{\infty} F_{\lambda} d\lambda \approx 1.31 \times 10^{-9} \text{ erg cm}^{-2} \text{ s}^{-1}$, of which the PAH component contributes $\sim 10\%$.⁶ This results in a total IR luminosity of $L_{\text{IR}} \approx 2.75 L_{\odot}$ at $d = 260 \text{ pc}$ and a ratio of the IR luminosity to the stellar luminosity of $L_{\text{IR}}/L_{\star} \approx 0.13$. Previous studies estimated $L_{\text{IR}}/L_{\star} \sim 0.14$ (Sheret et al. 2004) or ~ 0.15 (Sylvester et al. 1996), in close agreement with our estimate.

The best-fit model predicts that the peak radius of the dust spatial distribution in the HD 34700 disk is located at $r_{\text{p}} \approx 100 \text{ AU}$ from the central star. The peak radius r_{p} derived here can be compared with the inner radius (i.e., r_{min}) of the disk models proposed in the literature which assume a simple power-law dust spatial distribution and a peak distribution at r_{min} . Sylvester et al. (1996) and Dent et al. (2005) derived $r_{\text{min}} \approx 24\text{--}46 \text{ AU}$ (at $d \approx 55 \text{ pc}$) and $\lesssim 30 \text{ AU}$ (at $d \approx 125 \text{ pc}$), respectively. If we scale them to those at $d = 260 \text{ pc}$, our estimate is consistent with the former but is slightly larger than the latter.

Using the power-law size distribution and the spatial distribution of the dust (see Equation (2)), we estimate the total dust mass in the disk to be $M_{\text{dust}} \approx 21.9 M_{\oplus}$. There have been various estimates of the dust mass of the HD 34700 disk (e.g., see Zuckerman et al. 1995, Coulson et al. 1998, Sheret et al. 2004, Dent et al. 2005). Although these previous studies adopted different distances to HD 34700, ranging from $d \approx 60 \text{ pc}$ to $d \gtrsim 180 \text{ pc}$, the derived dust mass ranges from $M_{\text{dust}} \approx 7$ to $\sim 30 M_{\oplus}$ after scaling to $d = 260 \text{ pc}$ (i.e., $M_{\text{dust}} \propto d^2$), which overlaps with our estimate.

We calculate the equilibrium temperature, $T(r, a)$, of porous dust as a function of the radial distance r from the star and grain size a (see Figure 5(a)). The temperature decreases with increasing grain size⁷ and distance from the star. Figure 5(b) shows the equilibrium dust temperatures as a function of dust size at specific distances ($r = 20, 25$, and 100 AU). At $r = 25 \text{ AU}$, we see a sudden temperature drop around $a \approx 30 \mu\text{m}$. This is caused by the ice sublimation at $T \approx 120 \text{ K}$: porous dust larger than $a \sim 30 \mu\text{m}$ attains $T \approx 120 \text{ K}$ at $r \approx 25 \text{ AU}$. When the silicate and carbonaceous subgrains acquire an ice mantle at $T < 120 \text{ K}$, their aggregates will be less absorptive and therefore attain a lower equilibrium temperature.

The location where dust grains have low enough temperatures to capture volatile molecules to form ice mantles is called the “snowline.” The snowline plays an important role in the PAH chemistry since free-flying PAHs will condense onto the ice mantles. As shown in Fig-

⁶In contrast, in the Galactic diffuse ISM the PAH component accounts for $\sim 1/3$ of the total IR luminosity.

⁷For large grains with $a \gtrsim 100 \mu\text{m}$, they emit like a blackbody and their temperatures are independent of grain size.

ure 5(a), the transition from non-icy grains to icy grains occurs at different distances from the star for grains of different sizes: for smaller grains, the “snowline” is further away from the star, and by $r \approx 80$ AU all grains become ice-coated. For simplicity, in the following, we adopt $r = 25$ AU as the snowline of the HD 34700 disk.

Although the observed SED is closely reproduced by our best-fit model, there could exist some flexibilities for the model parameters. We briefly describe here the robustness of our model and refer to Li & Lunine (2003a), who explicitly discussed all the parameters of the porous dust model for disks (see their Section 4.1 for details). First, we examine the adopted dust parameters a_{\min} , a_{\max} , and P while other parameters remain unchanged. We differ a_{\min} between $0.1 \mu\text{m}$ and $10 \mu\text{m}$. While models with a large a_{\min} ($\sim 10 \mu\text{m}$) emit too little in the mid-IR at $\lambda \lesssim 40 \mu\text{m}$, those with a small a_{\min} ($\sim 0.1 \mu\text{m}$) deviate the fit at the mid- and far-IR. Similarly, by varying a_{\max} from $100 \mu\text{m}$ up to 1 cm , we find that sufficiently large grains ($\gtrsim 0.1 \text{ cm}$) are necessary for reproducing the observed submm emission. The models with $1000 \mu\text{m} \lesssim a_{\max} \lesssim 1 \text{ cm}$ produce almost identical SEDs. As a_{\max} decreases, the total dust mass (M_{dust}) decreases by a factor of ~ 3 at most. The porosity P is degenerate with a_{\min} and r_{\min} since decreasing a_{\min} or r_{\min} or increasing P has the same effect of increasing the dust temperature. However, a porosity in the range of $0.80 \lesssim P \lesssim 0.90$ is expected for dust aggregates formed through coagulation as demonstrated both theoretically (Cameron & Schneck 1965) and experimentally (Blum & Wurm 2008). Moreover, a porosity of $P \simeq 0.90$ is consistent with the mean mass density of cometary nuclei for which the ice-coated dust aggregates are plausible building blocks (see Greenberg & Li 1999). It is worth noting that the fluxes calculated from models with $0.8 \lesssim P \lesssim 0.95$ for the HD 34700 disk agree with each other within $\lesssim 25\%$.

We also examine the dust spatial distribution parameters r_p and γ which are not readily constrained due to the lack of spatial resolution of the disk. We find that models with small r_p ($\lesssim 80$ AU) would emit too much around $\lambda \sim 10 \mu\text{m}$ due to the silicate emission feature, while models with large r_p ($\gtrsim 200$ AU) fail to explain the far-IR/submm emission. The $80 \text{ AU} \lesssim r_p \lesssim 150 \text{ AU}$ models produce reasonable fits, with M_{dust} varying by a factor of ~ 2 at most. We also find that varying γ ($1.0 \lesssim \gamma \lesssim 3.5$; combined with r_p) does not affect the model-fit significantly. In summary, although different combinations of model parameters may be able to explain the observed SED, the underlying results do not change. The estimate of M_{dust} is most vulnerable (by a factor of ~ 3 at most), while the other estimates (e.g., \dot{M}_{RP} and \dot{M}_{PR} in Section 5.5) vary within $\sim 20\%$.

5. Discussion

5.1. PAHs in the HD 34700 Disk

As mentioned in Section 4, due to the single-photon heating nature of PAHs, the total mass of PAHs in the disk (M_{PAH}) required to reproduce the observed PAH emission is simply scaled by U , the starlight intensity. However, we cannot constrain U (which is inverse proportional to r^2 , i.e., $U(r) \propto (r/\text{AU})^{-2}$) since the HD 34700 disk has not been spatially resolved and hence we do not have any prior knowledge of the spatial distribution of PAHs. One may derive $M_{\text{PAH}} \approx 2.83 \times 10^{-4} M_{\oplus}$ by locating all PAHs at $r = 25 \text{ AU}$,⁸ the location of the snowline in the HD 34700 disk. Beyond the snowline, grains start to be ice-coated (see Figure 5), and the free-flying PAHs will condense onto the ice mantles and will not be excited to emit at the observed PAH features.

Even with $M_{\text{PAH}} \approx 2.83 \times 10^{-4} M_{\oplus}$ for $r = 25 \text{ AU}$, the PAH-to-dust mass ratio is only $M_{\text{PAH}}/M_{\text{dust}} \approx 1.3 \times 10^{-5}$,⁹ much smaller than that of the Galactic diffuse ISM ($M_{\text{PAH}}/M_{\text{dust}} \approx 0.05$, Li & Draine 2001, Draine & Li 2007). The deficit of PAHs relative to dust has previously been reported for debris disks (e.g., see Li & Lunine 2003a, Thi et al. 2013). However, the derived PAH-to-dust mass ratio may not reflect the actual PAH-to-dust mass ratio in the HD 34700 disk as there could be a substantial amount of PAHs in the disk beyond the snowline.

The minor features at 3.43 , 6.89 , and $7.23 \mu\text{m}$ shown in the HD 34700 disk reveal that the PAH molecules very likely have aliphatic sidegroups, although the $3.43 \mu\text{m}$ feature could also be due to anharmonicity and/or superhydrogenation of the aromatic C–H stretch (Barker et al. 1987, Bernstein et al. 1996). Let $I_{3.4}$ and $I_{3.3}$ be the observed intensities of the $3.43 \mu\text{m}$ and $3.3 \mu\text{m}$ emission features, respectively. For the HD 34700 disk, the *IRTF*/SpeX spectrum gives $I_{3.4}/I_{3.3} \approx 0.49$. Let $A_{3.4}$ and $A_{3.3}$ be the band strengths of the aliphatic and aromatic C–H bonds, respectively. Yang et al. (2013) calculated $A_{3.4}/A_{3.3} \approx 1.76$. By assuming that the $3.43 \mu\text{m}$ emission is exclusively due to aliphatic C–H (i.e., neglecting anharmonicity and superhydrogenation), we can place an upper limit on the ratio of the number of C atoms in aliphatic sidegroups to that in aromatic benzene rings: $N_{\text{C,aliph}}/N_{\text{C,arom}} \approx 0.3 \times$

⁸This means that most of the PAHs are concentrated within $r \sim 25 \text{ AU}$ corresponding to an angular size of $\theta \approx 0''.1$ at a distance of $d \sim 260 \text{ pc}$. Future IR observations with a sub-arcsecond spatial resolution such as the *Near Infrared Camera* (NIRCam) onboard the *James Webb Space Telescope* will shed light on the spatial distribution of dust and PAHs in debris disks.

⁹In HD 34700, the fractional IR luminosity ($L_{\text{PAH}}/L_{\text{IR}} \sim 10\%$, see Section 4) emitted by PAHs is much higher than the PAH-to-dust mass ratio. This is because PAHs are closer to the central star and also much more absorptive than the bulk porous dust.

$(I_{3.4}/I_{3.3}) \times (A_{3.3}/A_{3.4}) \approx 0.22$. It is assumed here that one aliphatic C atom corresponds to 2.5 aliphatic C–H bonds and one aromatic C atom corresponds to 0.75 aromatic C–H bond (see Li & Draine 2012). Similarly, we can place an upper limit of $N_{\text{C,aliph}}/N_{\text{C,arom}} \approx 0.14$ from the ratio of the observed intensity of the $6.89\,\mu\text{m}$ feature to that of the $7.7\,\mu\text{m}$ feature ($I_{6.89}/I_{7.7} \approx 0.064$; see Section 3 of Li & Draine 2012 for details).

It is not clear why PAHs are rarely seen in debris disks. This may be related to the disk structure and the stellar age.

There exists evidence that most of the protoplanetary disks in which the PAH emission features have been detected have a flaring disk geometry (Meeus et al. 2001, Acke & van den Ancker 2004). A common interpretation for this is that flared disks intercept more stellar radiation than flat ones, especially at large distances from the central star; the PAH emission originates in the surface layers of a flared disk, where PAHs are directly exposed to starlight (Chiang & Goldreich 1997, Meeus et al. 2001, Acke & van den Ancker 2004, Habart, Natta, & Krügel 2004). It is not clear if this scenario applies to the HD 34700 disk as it is not spatially resolved.

If the PAHs seen in debris disks originate from the outgassing of cometary bodies (i.e., the sublimation of the icy mantles coated on cometary grains onto which PAHs have condensed during the protostellar dense cloud phase, see Li & Lunine 2003a), it is more likely to see PAHs in relatively young debris disks as they are subject to massive bombardment by cometary bodies (Chyba et al. 1994). With an age of a few tens of mega-years (Torres 2004), the HD 34700 disk is probably still in the heavy bombardment phase as it lasted more than 500 mega-years in our early solar system (Chyba et al. 1994).

5.2. PAH Destruction

A PAH molecule is subjected to photodissociation upon absorbing an energetic photon. During this process, PAHs, preferentially small PAHs, might lose a hydrogen atom, a hydrogen molecule, or an acetylene molecule (C_2H_2), which eventually results in the destruction of a PAH molecule. Following Li & Lunine (2003a), we have calculated the photodestruction rates (k_{des}) for the PAHs in the HD 34700 disk assuming that a PAH molecule is destroyed through the C_2H_2 ejection. Figure 6 shows the photodestruction timescales ($\tau_{\text{des}} \equiv 1/k_{\text{des}}$) at given distances ($r = 10, 15$, and $25\,\text{AU}$). During the lifetime of HD 34700 ($\tau_{\star} \approx 10\,\text{Myr}$), PAHs with a size of $\lesssim 4.1\,\text{\AA}$ (corresponding to PAHs with ~ 35 carbon atoms) are likely to be photodestroyed. Against the complete removal of such small PAHs in the HD 34700 disk, these PAHs have to be replenished continuously, which is indeed required to account

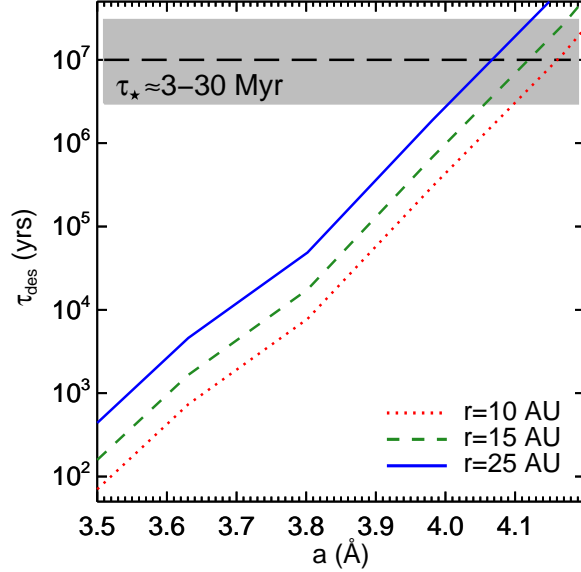


Fig. 6.— Photodestruction timescales (τ_{des}) for PAHs at $r = 10$ AU (dotted line), 15 AU (dashed line), and 25 AU (solid line) as a function of size. The age of HD 34700 (τ_{\star}) is rather uncertain, ranging from ~ 3 Myr up to several tens of Myrs. The age range ($\tau_{\star} \approx 3 - 30$ Myr) is designated by the **shaded** region with the representative value of $\tau_{\star} \approx 10$ Myr plotted as a long-dashed line.

for the observed PAH emission. Assuming the PAHs in the HD 34700 disk follow the same spatial distribution as porous dust (see Equation (2)) but with a cutoff at $r = 25$ AU, we estimate the PAH mass replenishment rate to be $\dot{M}_{\text{PAH}} \approx 4.5 \times 10^{-9} M_{\oplus} \text{yr}^{-1}$ taking only photodestruction into account (see also Section 5.5).

5.3. Radiation Pressure

Small dust in a debris disk is continuously expelled outward due to the RP against the gravitational force (Backman & Paresce 1993). Following the approach described in Section 4.3 of Li & Lunine (2003a), we derive the ratio of the radiative force to the gravitational force (β_{RP}) as a function of grain size. Both the RP and the gravitational force are inversely proportional to r^2 , as a result, β_{RP} is independent of the distance from the central star.

We find that grains smaller than $\sim 20\text{--}40 \mu\text{m}$ have $\beta_{\text{RP}} \gtrsim 1$ (see Figure 7). This indicates that grains with a radius smaller than $\sim 40 \mu\text{m}$ ($\sim 20 \mu\text{m}$ for icy grains) will be blown out due to RP. Moreover, assuming that the gas drag is not overwhelming which is true for debris disks, even larger grains ($\sim 40\text{--}80 \mu\text{m}$) could be pushed outward (see Figure 7) because dust

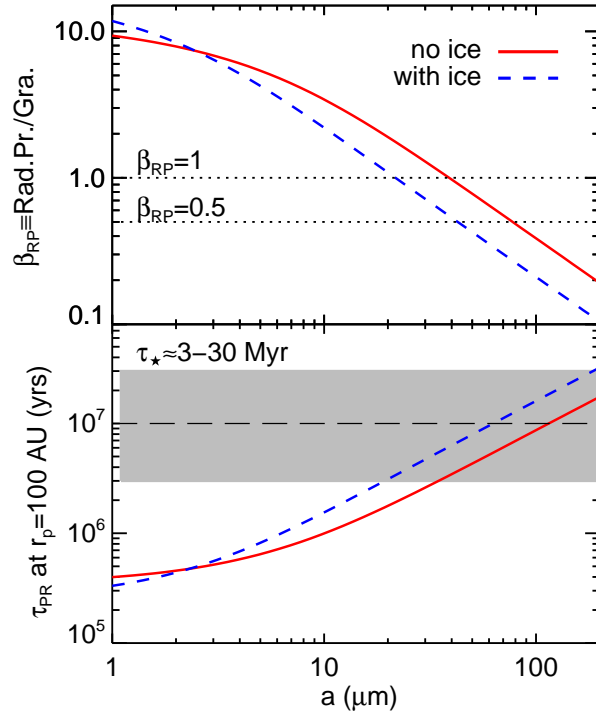


Fig. 7.— Ratio of the radiative force to the gravitational force (β_{RP} , top panel) and the Poynting–Robertson drag timescale (τ_{PR} , bottom panel) for ice-free porous dust ($P = 0.9$: solid line) and ice-coated porous dust ($P' \approx 0.73$, dashed line) at $r = 100 \text{ AU}$ (note $\tau_{\text{PR}} \propto r^2$). The stellar age (τ_\star) is marked in the same way as Figure 6.

particles released from parent bodies at periastron only need $\beta_{\text{RP}} = 0.5$ for ejection (Burns et al. 1979).

Unlike dust grains, the β_{RP} ratio for PAHs is not sensitive to their sizes as they are in the Rayleigh limit (see Li 2009a). We estimate $\beta_{\text{RP}} \approx 35$ for the PAHs in the HD 34700 disk.

5.4. Poynting–Roberson Drag

Dust grains can migrate inward due to the Poynting–Roberson (PR) drag (Backman & Paresce 1993). We calculate the PR drag timescale (τ_{PR}), which is a function of grain size and the distance (r) from the star. Note that, unlike the RP ejection, the PR drag is proportional to r^2 .

At the peak distance of $r_{\text{p}} \approx 100$ AU, grains smaller than $\sim 50\text{--}100\ \mu\text{m}$ have a PR lifetime shorter than the age of HD 34700 (assuming $\tau_{\star} \approx 10$ Myr; see Figure 7). The closer dust grains are located to the star, the bigger grains will be gradually accreted to the central star. For PAHs, we estimate $\tau_{\text{PR}} \approx 6000$ yr for PAHs at $r = 25$ AU, which is independent of their sizes for the same reason as for β_{RP} .

5.5. Dominant Processes for the Removal of Dust and PAHs in the HD 34700 Disk

Taking into account the RP ejection, the PR drag, as well as the photodissociation of PAHs, we examine the removal of dust and PAHs in the HD 34700 disk as a function of their sizes and distance from the star. The RP timescale in the HD 34700 disk is estimated to be $\tau_{\text{RP}}(r) \approx 912 (r/100 \text{ AU})^{3/2}$ yr assuming that it is comparable to the local dynamical timescale $\tau_{\text{dyn}} = 2\pi/\Omega(r)$, where $\Omega(r)$ is the Keplerian frequency. For grains with $\beta_{\text{RP}} \gtrsim 0.5$ (i.e., $a \lesssim 80\ \mu\text{m}$), the RP timescale at a given distance is much smaller than the PR drag timescale (see Figure 7). Therefore, for these grains the RP expulsion is the dominant removal process over the entire disk. For larger grains (i.e., $a \gtrsim 80\ \mu\text{m}$), if the PR timescale $\tau_{\text{PR}}(a, r)$ is shorter than the stellar age τ_{\star} , the PR drag becomes an effective removal mechanism. At $r = 100$ AU, this applies to grains of $a \lesssim 100\ \mu\text{m}$ (see Figure 7). For grains at a larger distance from the star, the size range over which the PR drag is effective becomes narrower, and eventually, the PR drag no longer contributes to the dust removal beyond $r \sim 150$ AU.

Since the overall dust removal in the HD 34700 disk is dominated by the RP ejection, we calculate the RP dust mass-loss rate for our best-fit model. Following Equation (20) in Li & Lunine (2003a), we derive $\dot{M}_{\text{RP}} \approx 2.05 \times 10^{-4} M_{\oplus} \text{ yr}^{-1}$. Hence, $\sim 2000 M_{\oplus}$ of dust

has been removed during the lifetime of HD 34700. For comparison, the PR dust mass-loss rate integrated over the dust size distribution and over the entire disk is estimated to be $\dot{M}_{\text{PR}} \approx 1.78 \times 10^{-7} M_{\oplus} \text{yr}^{-1}$.

In the same manner as for dust grains, we estimate the PAH mass loss rate due to the RP expulsion to be $\dot{M}_{\text{RP}}(\text{PAH}) \approx 2.92 \times 10^{-6} M_{\oplus} \text{yr}^{-1}$. Note that PAHs are also subject to photodissociation (see Section 5.2). We found that the RP timescale is much shorter than the photodestruction timescale except for the smallest PAHs ($a \approx 3.5\text{--}3.6 \text{ \AA}$). The PAH mass loss rate via the RP expulsion (\dot{M}_{RP}) yields that $\sim 30 M_{\oplus}$ of PAH molecules have been removed from the disk or have been replenished to maintain the current PAH abundance during the 10 Myr lifetime of HD 34700.

It is interesting to note that the PAH-to-dust mass-loss ratio, $\dot{M}_{\text{RP}}(\text{PAH})/\dot{M}_{\text{RP}}(\text{dust}) \approx 1.4 \times 10^{-2}$, is about three order of magnitudes higher than the PAH-to-dust mass ratio of $M_{\text{PAH}}/M_{\text{dust}} \approx 1.3 \times 10^{-5}$ (see Section 5.1). This is because only grains with $a \lesssim 80 \mu\text{m}$ will be ejected by the RP expulsion (see Figure 7) and with a best-fit dust size distribution of $dn/da \propto a^{-3.5}$ (see Section 4), the total dust mass in the HD 34700 disk is dominated by much larger grains. Thus, only a small mass fraction of the dust is subject to the RP expulsion, whereas PAHs of all sizes have been removed or replenished.

The high removal rates of small dust and PAHs derived above require an efficient replenishment probably provided by the outgassing and collisions of planetesimals, asteroidal, and cometary bodies to contain a stable amount of small grains and PAHs in the disk (Backman & Paresce 1993, Wyatt 2008, Kiefer et al. 2014). In particular, as PAHs have been detected in interplanetary dust particles, comets, and meteorites (e.g., see Li 2009b for overview), cometary origin of PAHs in the HD 34700 disk is plausible. By systematically studying all debris disks with detected PAH features, we will (hopefully) be able to constrain the origin of PAHs and dust in debris disks (J. Y. Seok & A. Li, 2015, in preparation).

6. Summary

The HD 34700 disk is one of the few debris disks that show prominent PAH emission in their IR spectra. We have modeled the PAH emission of the HD 34700 disk as well as its entire SED from the near-IR up to submm/mm wavelength regime. The stellar RP and Poynting–Robertson drag quickly remove the dust and PAHs in the HD 34700 disk, implying that they must have been replenished continuously to maintain their current abundances.

The major PAH features at 3.3, 6.2, 7.7, 8.6, and 11.3 μm (as well as the minor features at 3.43, 6.89, and 7.23 μm) are present in the IR spectra, indicating the presence of a mixture

of neutral and ionized PAHs (with aliphatic sidegroups) in the disk. By comparing the photoionization and electron recombination timescales, it is found that the PAHs in the inner disk are likely to be ionized while those in the outer disk are to be neutral or negatively charged. Also, at a given distance from the star, smaller PAHs are more likely to be neutral whereas larger PAHs are more likely to be charged. Hence, one would expect a mixture of neutral and ionized PAHs in the HD 34700 disk.

Adopting a log-normal size distribution for the PAHs, the HD 34700 disk is in favor of smaller PAHs ($a_0 = 3.5 \text{ \AA}$ and $\sigma = 0.3$) compared to that of the diffuse ISM. This is supported by the prominent $3.3 \mu\text{m}$ PAH feature, which is indicative of small, neutral PAHs. The $3.43 \mu\text{m}$ feature commonly attributed to aliphatic C–H stretch allows us to place an upper limit of ~ 0.22 on the ratio of C atoms in aliphatic sidegroups to that in aromatic benzene rings. The $6.89 \mu\text{m}$ feature, an aliphatic C–H deformation band, derives the ratio of aliphatic C atoms to aromatic C atoms to be ~ 0.14 .

The total IR luminosity of $L_{\text{IR}} \approx 2.75 L_{\odot}$ is derived with a distance of $d = 260 \text{ pc}$. This leads to $L_{\text{IR}}/L_{\star} \approx 0.13$, and the PAH emission accounts for $\sim 10\%$ of the total L_{IR} . Our best fit model suggests that the dust spatial distribution peaks at $\approx 100 \text{ AU}$ and decreases outward with a power-law index of $\gamma \approx 2$. Taking the disk geometry into account, the total dust mass in the disk is estimated to be $M_{\text{dust}} \approx 21.9 M_{\oplus}$. Porous grains larger than $\sim 30 \mu\text{m}$ attain an equilibrium temperature of $T \lesssim 120 \text{ K}$ at $r \approx 25 \text{ AU}$, indicating that ice mantles on these grains begin to develop at $r \approx 25 \text{ AU}$. Therefore, $r = 25 \text{ AU}$ is regarded as the “snowline” in the HD 34700 disk.

Without any prior knowledge of the PAH spatial distribution, the observed PAH emission yields a total mass of $M_{\text{PAH}} \approx 4.53 \times 10^{-7} (r/\text{AU})^2 M_{\oplus}$ if one assumes that all the PAHs are at a distance of r from the central star. As free-flying PAHs will easily condense onto the ice mantles beyond the snowline, an upper limit of $M_{\text{PAH}} \approx 2.83 \times 10^{-4} M_{\oplus}$ is derived for $r = 25 \text{ AU}$. This results in a PAH-to-dust mass ratio of $M_{\text{PAH}}/M_{\text{dust}} \approx 1.3 \times 10^{-5}$, indicating a deficiency of PAHs in debris disks compared with the diffuse ISM.

The photodissociation of PAH molecules occurs continuously by absorbing an energetic photon, and small PAHs ($\lesssim 4.1 \text{ \AA}$) are likely to have been photo-destroyed during the lifetime of HD 34700 ($\tau_{\star} \approx 10 \text{ Myr}$). We calculate the PAH mass replenishment rate to be $\approx 4.5 \times 10^{-9} M_{\oplus} \text{ yr}^{-1}$ due to photodissociation.

The stellar RP dominates the dust and PAH removal in the HD 34700 disk. Due to the RP together with Poynting–Robertson drag, $\sim 2000 M_{\oplus}$ of dust has been removed during the $\sim 10 \text{ Myr}$ lifetime of HD 34700. Similarly, $\sim 30 M_{\oplus}$ of PAHs has been removed out of the disk. Collisions and/or sublimations of planetesimals, asteroids, and comets are the likely

origin of the dust and PAH replenishment.

We thank L. D. Keller, S. Wang and the anonymous referee for their very helpful suggestions. We are supported in part by NSF AST-1109039, NNX13AE63G, NSFC 11173019, and the University of Missouri Research Board.

REFERENCES

- Acke, B., & van den Ancker, M. E. 2004, *A&A*, 426, 151
- Acke, B., Bouwman, J., Juhász, A., et al. 2010, *ApJ*, 718, 558
- Allamandola, L.J., Tielens, A.G.G.M., & Barker, J.R. 1985, *ApJ*, 290, L25
- Arellano Ferro, A., & Giridhar, S. 2003, *A&A*, 408, L29
- Backman, D.E., & Paresce, F. 1993, in *Protostars and Planets III*, ed. E.H. Levy & J.I. Lunine (Tucson: Univ. Arizona Press), 1253
- Bakes, E. L. O., & Tielens, A. G. G. M. 1994, *ApJ*, 427, 822
- Barker, J.R., Allamandola, L.J., & Tielens, A.G.G.M. 1987, *ApJ*, 315, L61
- Berné, O., Joblin, C., Fuente, A., & Ménard, F. 2009, *A&A*, 495, 827
- Bernstein, M.P., Sandford, S.A., & Allamandola, L.J. 1996, *ApJ*, 472, L127
- Blum, J., & Wurm, G. 2008, *ARA&A*, 46, 21
- Brooke, T. Y., Tokunaga, A. T., & Strom, S. E. 1993, *AJ*, 106, 656
- Burns, J.A., Lamy, P.L., & Soter, S. 1979, *Icarus*, 40, 1
- Cameron, A. G. W., & Schneck, P. B. 1965, *Icarus*, 4, 396
- Chen, C.H., Sargent, B.A., Bohac, C., et al. 2006, *ApJS*, 166, 351
- Chiang, E. I., & Goldreich, P. 1997, *ApJ*, 490, 368
- Chyba, C. F., Owen, T. C., & Ip, W.-H. 1994, in *Hazards due to Comets and Asteroids*, ed. T. Gehrels, M.S. Matthews, & A.M. Schumann (Tucson: Univ. Arizona Press), 9
- Coulson, I. M., & Walther, D. M. 1995, *MNRAS*, 274, 977

- Coulson, I. M., Walther, D. M., & Dent, W. R. F. 1998, MNRAS, 296, 934
- Dent, W. R. F., Greaves, J. S., & Coulson, I. M. 2005, MNRAS, 359, 663
- Draine, B. T., & Lee, H. M. 1984, ApJ, 285, 89
- Draine, B.T., & Li, A. 2001, ApJ, 551, 87
- Draine, B.T., & Li, A. 2007, ApJ, 657, 810
- Furlan, E., Hartmann, L., Calvet, N., et al. 2006, ApJS, 165, 568
- Geers, V. C., Augereau, J.-C., Pontoppidan, K. M., et al. 2005, Protostars and Planets V (LPI Contrib. 1286; Houston: LPI), 8409
- Greenberg, J. M., & Li, A. 1999, Planet. Space Sci., 47, 787
- Habart, E., Natta, A., & Krügel, E. 2004, A&A, 427, 179
- Habart, E., Natta, A., Testi, L., & Carbillet, M. 2006, A&A, 449, 1067
- Ishihara, D., Onaka, T., Kataza, H., et al. 2010, A&A, 514, 1
- Joblin, C. 2015, Highlights of Astronomy, 16, 699
- Joblin, C., Tielens, A.G.G.M., Allamandola, L.J., & Geballe, T.R. 1996, ApJ, 458, 610
- Keller, L. D., Sloan, G. C., Forrest, W. J., et al. 2008, ApJ, 684, 411
- Kiefer, F., Lecavelier des Etangs, A., Boissier, J., et al. 2014, Nature, 514, 462
- Kurucz, R. L. 1979, ApJS, 40, 1
- Léger, A., & Puget, J. 1984, A&A, 137, L5
- Li, A. 2009a, in Small Bodies in Planetary Sciences (Lecture Notes in Physics vol. 758), ed. I. Mann, A. Nakamura, & T. Mukai, Springer, Chapter 6, 167
- Li, A. 2009b, in Deep Impact as a World Observatory Event: Synergies in Space, Time, and Wavelength, ed. H. U. Käuffl & C. Sterken, 161
- Li, A., & Draine, B.T. 2001, ApJ, 554, 778
- Li, A., & Draine, B.T. 2012, ApJ, 760, L35
- Li, A., & Greenberg, J.M. 1998, A&A, 331, 291

- Li, A., & Lunine, J.I. 2003a, ApJ, 594, 987
- Li, A., & Lunine, J.I. 2003b, ApJ, 590, 368
- Mathis, J. S., Mezger, P. G., & Panagia, N. 1983, A&A, 128, 212
- Meeus, G., Waters, L. B. F. M., Bouwman, J., et al. 2001, A&A, 365, 476
- Mendigutà, I., Mora, A., Montesinos, B., et al. 2012, A&A, 543, A59
- Peeters, E. 2014, in IAU Symp. 297, The Diffuse Interstellar Bands, ed. J. Cami & N.L.J. Cox, (Cambridge: Cambridge Univ. Press), 187
- Peeters, E., Hony, S., Van Kerckhoven, C., et al. 2002, A&A, 390, 1089
- Rouleau, F., & Martin, P. G. 1991, ApJ, 377, 526
- Schütz, O., Meeus, G., Sterzik, M. F., & Peeters, E. 2009, A&A, 507, 261
- Sheret, I., Dent, W. R. F., & Wyatt, M. C. 2004, MNRAS, 348, 1282
- Siebenmorgen, R., Prusti, T., Natta, A., & Müller, T. G. 2000, A&A, 361, 258
- Sloan, G. C., Keller, L. D., Forrest, W. J., et al. 2005, ApJ, 632, 956
- Smith, T. L., Clayton, G. C., & Valencic, L. 2004, AJ, 128, 357
- Sterzik, M. F., Melo, C. H. F., Tokovinin, A. A., & van der Blik, N. 2005, A&A, 434, 671
- Sylvester, R. J., Skinner, C. J., & Barlow, M. J. 1997, MNRAS, 289, 831
- Sylvester, R. J., Skinner, C. J., Barlow, M. J., & Mannings, V. 1996, MNRAS, 279, 915
- Thi, W., Pinte, C., Pantin, E., et al. 2013, A&A, 561, A50
- Tielens, A. G. G. M. 2008, ARA&A, 46, 289
- Torres, G. 2004, AJ, 127, 1187
- van Boekel, R., Waters, L. B. F. M., Dominik, C., et al. 2004, A&A, 418, 177
- van den Ancker, M. 1998, A&A, 154, 145
- Walker, H. J., & Wolstencroft, R. D. 1988, PASP, 100, 1509
- Weinberger, A. J., & Becklin, E. E. 2005, Protostars and Planets V (LPI Contrib. 1286; Houston: LPI), 8561

Weingartner, J. C., & Draine, B. T. 2001, *ApJS*, 134, 263

Wyatt, M. C. 2008, *ARA&A*, 46, 339

Yang, X. J., Glaser, R., Li, A., & Zhong, J. X. 2013, *ApJ*, 776, 110

Zuckerman, B., Forveille, T., & Kastner, J.H. 1995, *Nature*, 373, 494